

# High-Resolution CISS MR Imaging With and Without Contrast for Evaluation of the Upper Cranial Nerves Segmental Anatomy and Selected Pathologic Conditions of the Cisternal Through Extraforaminal Segments

Ari M. Blitz, MD<sup>a,\*</sup>, Leonardo L. Macedo, MD<sup>b</sup>, Zachary D. Chonka, MD<sup>a</sup>, Ahmet T. Ilica, MD<sup>a</sup>, Asim F. Choudhri, MD<sup>c</sup>, Gary L. Gallia, MD, PhD<sup>d</sup>, Nafi Aygun, MD<sup>a</sup>

## KEYWORDS

- High-resolution MR imaging • Cranial nerves • Segmental classification • CISS
- Upper cranial nerves

## KEY POINTS

- High-resolution isotropic three-dimensional (3D) magnetic resonance imaging acquisition relying heavily on constructive interference in the steady state (CISS) with and without contrast has largely replaced 2D techniques previously used for the evaluation of the cranial nerves (CNs) at the authors' institution and allows for high-contrast evaluation of the CNs along a greater portion of their extent than was previously possible.
- The cisternal and dural cave segments of the upper CNs, with the possible exception of the fourth cranial nerve, are well evaluated with noncontrast CISS.
- The interdural and foraminal segments of the CNs are revealed after the administration of intravenous contrast.
- The proximal extraforaminal segments of the CNs are often well visualized on 3D high-resolution imaging with CISS.
- Evaluation for pathologic contrast enhancement in segments of the upper CNs which were previously not well seen, and on a scale previously not well depicted, is now possible with high-resolution 3D technique.

<sup>a</sup> Division of Neuroradiology, The Russell H. Morgan Department of Radiology and Radiologic Science, The Johns Hopkins Hospital, Phipps B-100, 600 North Wolfe Street, Baltimore, MD 21287, USA; <sup>b</sup> Cedimagem/Alliar Diagnostic Center, 150- Centro, Juiz de Fora, Minas Gerais 36010-600, Brazil; <sup>c</sup> Department of Radiology, University of Tennessee Health Science Center, Le Bonheur Neuroscience Institute, Le Bonheur Children's Hospital, 848 Adams Avenue-G216, Memphis, TN 38103, USA; <sup>d</sup> Department of Neurosurgery, Neurosurgery Skull Base Surgery Center, The Johns Hopkins Hospital, Phipps 101, 600 North Wolfe Street, Baltimore, MD 21287, USA

\* Corresponding author.

E-mail address: Ablitz1@jhmi.edu

## INTRODUCTION

Although long used for the evaluation of the course of the cranial nerves (CNs) within the subarachnoid space,<sup>1</sup> the recognition of the utility of enhancement on postcontrast constructive interference in the steady state (CISS) imaging allows for the evaluation of the remainder of the extended course of the CNs once they exit the subarachnoid space.<sup>2</sup> In this article, the authors review the recent literature on the evaluation of the CNs with CISS and analogous sequences and describe the use of such techniques for the evaluation through the extraforaminal segments. In many instances, such techniques enable visualization of nearly the entire course of many of the upper CNs, and the relevant anatomy is described here following the segmental classification suggested in the article by Blitz, Choudhri, Chonka and colleagues within this issue (**Box 1**).

CISS imaging combines true and reversed fast imaging in steady state precession (FISP) imaging to allow for high-signal, high-spatial resolution imaging with suppression of banding artifacts caused by unbalanced imaging gradients and field inhomogeneities. CISS is a gradient echo technique, and images acquired have the appearance of strong T2 weighting but, in fact, demonstrate some degree of mixed weighting, which allows for the visualization of enhancement.<sup>3</sup>

The application of precontrast and postcontrast CISS imaging has several significant advantages over other techniques used for cranial nerve evaluation. CISS imaging allows for the acquisition of high spatial resolution isotropic 3-dimensional (3D) imaging in a clinically acceptable time period, allowing for the evaluation of the entirety of the skull base and posterior fossa at 0.6-mm isotropic resolution in less than 6 minutes. The addition of contrast allows for the depiction of the CNs in most segments with a single sequence, and it is simultaneously possible to assess for pathologic contrast enhancement. Unless otherwise noted, the images in this article were acquired on a 3T

Siemens Verio (Ehrlangen, Germany) with 0.6-mm isotropic resolution.

Although for the purposes of this discussion the authors use the nomenclature established in the article by Blitz, Choudhri, Chonka and colleagues within this issue for CN I to VI, CN I and CN II are properly considered tracts of the central nervous system (CNS) rather than true cranial nerves passing into the peripheral nervous system (PNS) and do not entirely conform to the same anatomic outline as CN III to VI. Although classically anatomists describe nerves from their point of origination to their destination, the mixed afferent and efferent components of several cranial nerves makes this challenging and potentially confusing. For the sake of simplicity, descriptions are given here following the nerve from their point of apparent origin at the brainstem peripherally into the extraforaminal components.

CN dysfunction may arise from pathologic conditions interrupting fiber bundles at any point from the CN nuclei to the end organ innervated by the nerve or often even from lesions within pathways that themselves innervate the CN nuclei. Lesions within the brain, cranial nerve nuclei, or fiber tracts, as they course to exit the brain and give rise to the CNs, are often associated with other signs of damage to the CNS<sup>4</sup>; such lesions are discoverable on imaging of the brain. Imaging of the cranial nerve nuclei and course of fibers within the substance of the brainstem itself is beyond the scope of this discussion, which focuses on imaging the CNs from their apparent origin at the surface of the brainstem through their exit from the skull base foramina. The interested reader will find excellent information on the location and course of the nuclear and fascicular segments, for instance, in the recent text by Naidich and colleagues.<sup>5</sup> Additionally, it is important to note that the entirety of the extraforaminal course of the upper CNs is complex and limited space precludes treatment of the entirety of the topic beyond some introductory remarks within this article.

## CN I: OLFACTORY NERVE

The olfactory nerve provides the sense of smell. The portions of the olfactory nerve visible on magnetic resonance (MR) imaging, namely, the olfactory bulb (OB) and olfactory tract (OT), are not components of a cranial nerve in the formal sense but rather a forward extension of the telencephalon,<sup>6</sup> more properly a tract of the CNS. As such, CN I does not follow the typical segmental pattern of CNs III to XII. For the purposes of this discussion, the authors define cisternal, foraminal, and extraforaminal segments. The olfactory tracts

### Box 1

#### Anatomic segments of the cranial nerves

- a. Nuclear
- b. Parenchymal fascicular
- c. Cisternal
- d. Dural cave
- e. Interdural
- f. Foraminal
- g. Extraforaminal

carry information on smell from the cisternal segment into the olfactory stria to the primary olfactory cortex located in the inferomedial aspect of the temporal lobe.

### **CN I.c (Cisternal): Anatomy**

CN I.c consists of the OB and the OT (**Fig. 1**). The OB sits above the cribriform plate and receives input from primary sensory neurons. The CNS-PNS transitional zone (TZ), located in the OB, is histologically distinct from that of the other CNs with a cell type, the ensheathing cell, not found in other CNs.<sup>7</sup> The OB is uniformly well visualized with CISS.<sup>8</sup> The neurons of the OB project posteriorly into the OT, which in turn extends posteriorly toward the brain. The OT is distinguished from the OB by a change in caliber, although the lack of a constant landmark has led to variability in identification between subjects and readers, hampering clinical evaluation and research. Some investigators advocate spin echo imaging rather than CISS for the evaluation of CN I.c to avoid artifacts in this region caused by air tissue interface.<sup>9</sup> In the authors' experience, diagnostic images of the anterior cranial fossa and paranasal sinuses can be obtained with CISS, with the significant advantage of also allowing for the assessment of contrast enhancement at a high spatial resolution. The quantitative size evaluation of OB and OT has demonstrated a correlation between OB/OT volume and olfactory function and an age-related decrease in OT volume.<sup>10,11</sup>

### **CN I.c: Selected Pathologic Conditions**

The congenital absence of CN I.c may be detected in patients as a component of Kallmann

syndrome.<sup>12,13</sup> Idiopathic olfactory loss is common, and patients with idiopathic olfactory loss demonstrate decreased OB volumes compared with normal controls.<sup>14</sup> Idiopathic anosmia can be a harbinger of Parkinson disease or Alzheimer disease.<sup>15–17</sup> Intra-axial and extra-axial tumors, most frequently meningioma, arising from the anterior skull base can result in anosmia. The vulnerability of the CN I.c to head trauma and post-traumatic olfactory dysfunction is well documented and also correlates with OB/OT size.<sup>18</sup>

### **CN I.f (Foraminal): Anatomy**

Up to 100 unmyelinated axons of the olfactory neuroepithelium form bundles (olfactory fila, the olfactory nerves proper) (see **Fig. 1B** white arrows) that extend intracranially through the openings of the cribriform plate before penetrating the dura. The numerous fila and the foramina in the cribriform plate are not reliably visualized with the current imaging resolution.

### **CN I.f: Selected Pathologic Conditions**

Traumatic injury to the cribriform plate resulting in loss of olfaction or cerebrospinal fluid (CSF) leak (CSF rhinorrhea) may occur in this region.

### **CN I.g (Extraforaminal): Anatomy**

The primary olfactory neurons are located in the neuroepithelium lining the superior nasal cavity.

### **CN I.g: Selected Pathologic Conditions**

The most common cause of anosmia involving the CN I.f is rhinosinusitis. The prototypical tumor of the CN I.g is esthesioneuroblastoma (olfactory

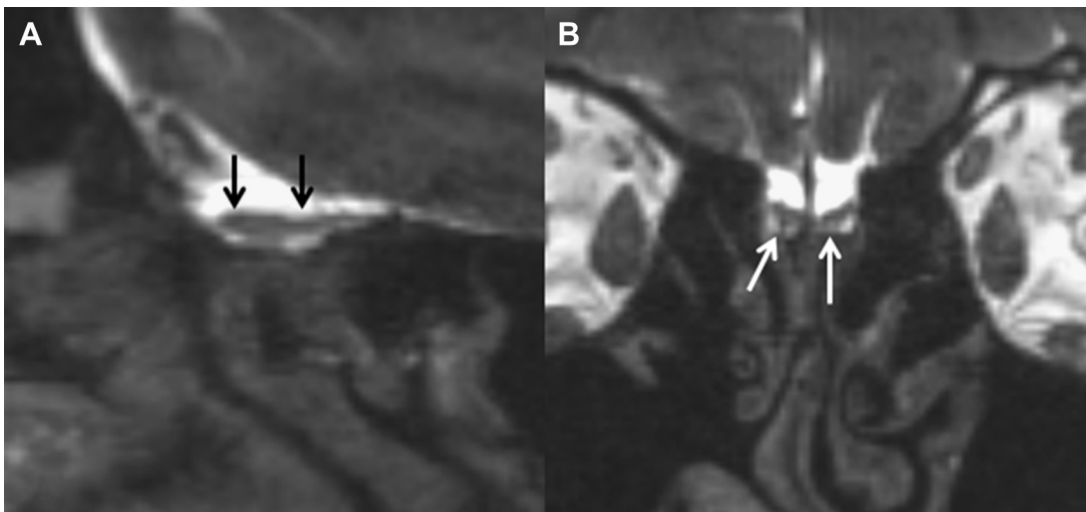


**Fig. 1.** (A) Sagittal CISS through the anterior cranial fossa demonstrates CN I.c with change in caliber noted between the OB and OT (black arrows). (B) On the coronal CISS image the olfactory fila (white arrows) joining the OB can be seen.

neuroblastoma), a rare lesion arising from the olfactory epithelium. A variety of tumors typically arise at the anterior skull base and in the region of CN I.g that commonly extend superiorly toward CN I.f. One of the main surgical considerations for malignant sinonasal tumors, including esthesioneuroblastomas, is whether the tumor has extended intracranially, which has an impact on the surgical approach as well as the prognosis.<sup>19</sup> CISS imaging provides a very accurate identification of the intracranial extension of disease and may allow the radiologist to detect the possibility of even a very small amount of intracranial tumor (Fig. 2).

### CN II: OPTIC NERVE

The optic nerve carries visual information from the globes into the intracranial compartment with a partial decussation of fibers at the optic chiasm and synapses at the lateral geniculate nucleus of the thalamus. As noted earlier, CN II is not a cranial nerve by the strict definition and does not conform to the segmental classification described. For the purposes of this discussion, the authors divide the nerve into cisternal, dural cave, foraminal, and extraforaminal segments. All of these CN II segments are intradural; however, the surrounding tissue signal varies from CSF to bone and fat. For

the purposes of this discussion, the authors define the attached component of CN II, the optic chiasm and optic tracts, as the fascicular component extending toward the lateral geniculate nucleus posterolaterally. As with the other CNs, the cisternal segment is limited to the component surrounded by the subarachnoid space on all sides. High-resolution CISS imaging provides superb anatomic detail regarding the location of CN II and its relationship to surrounding structures; postcontrast CISS imaging may also demonstrate subtle contrast enhancement within the nerve. For the assessment of intrinsic T2 signal abnormality, such as seen in optic neuritis, reliance on CISS technique alone is not advised, and imaging can be supplemented with spin echo–based T2 techniques.<sup>20</sup>

### CN II.c (Cisternal): Anatomy

For the purposes of this article, the cisternal anatomy of the optic nerves is limited to the portion of the prechiasmatic optic nerve, which extends from the posterior margin of the anterior clinoid process posteromedially to the optic chiasm (Fig. 3).

### CN II.c: Selected Pathologic Conditions

The most commonly encountered pathologic condition of CN II.c in adults is caused by extrinsic

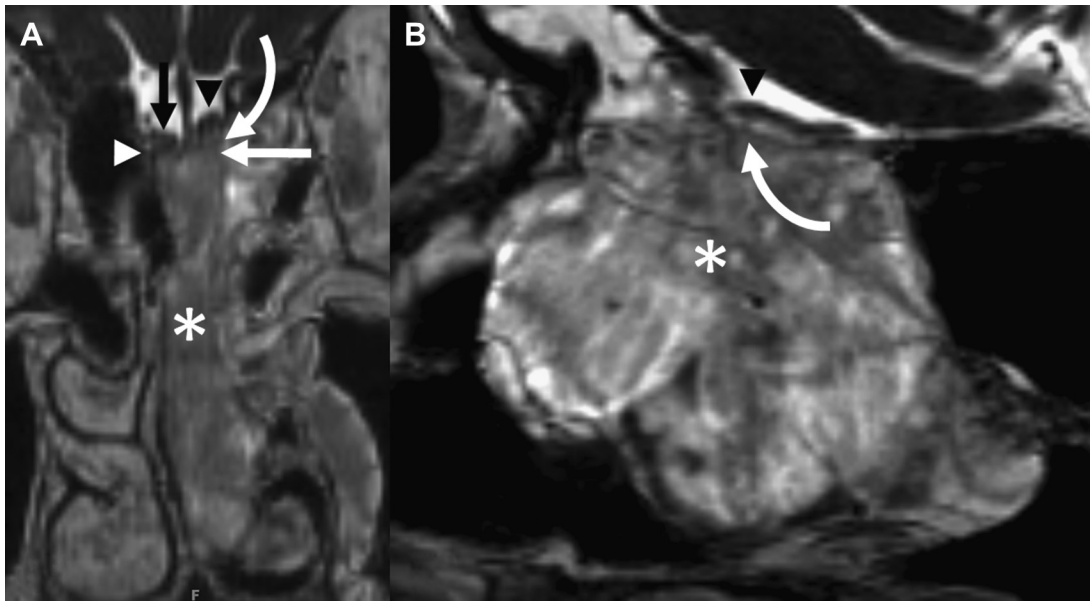


**Fig. 2.** (A) Coronal postcontrast CISS demonstrates an enhancing mass (asterisk) within the left nasal cavity traversing the nasal septum superiorly and extending to the level of the undersurface of the right cribriform plate (white arrowhead). On the left side, there is minimal soft tissue (curved arrow) interposed between the cribriform plate (white arrow) and OB (black arrowhead), which is subtly displaced superiorly compared with the contralateral side (black arrow). (B) Sagittal reformat again demonstrates 2 mm of extension across the left cribriform plate displacing the OB. Focal extension of esthesioneuroblastoma was noted in this location at the time of surgery.

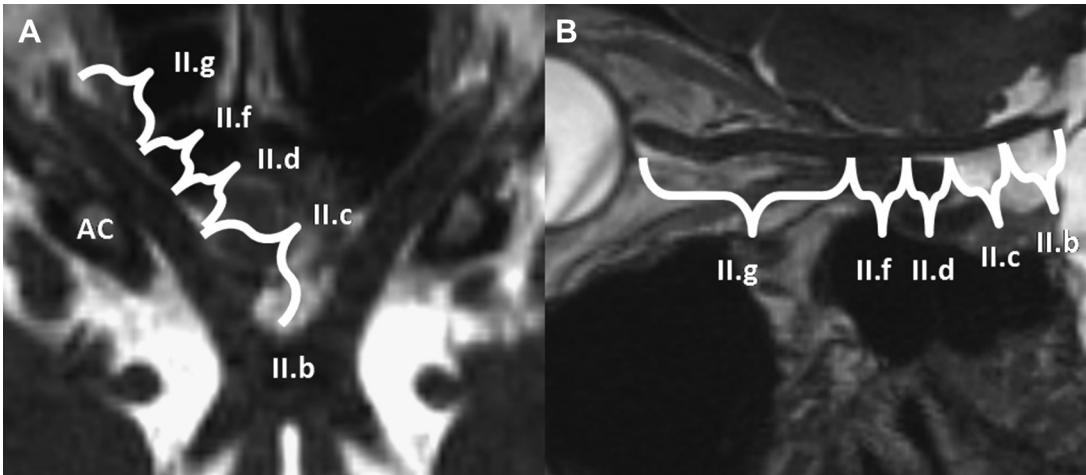


**Fig. 3.** (A) Axial postcontrast CISS demonstrates the posterior aspect of CN II.g within the orbital apex extending into the optic canals (CN II.f) and then passing intracranially as CN II.d medial to the anterior clinoid process (AC). CN II.c passes posteriorly to join the contralateral nerve as the first attached segment, the optic chiasm (II.b above). (B) In sagittal multi-planar reformat, the entirety of the nerve can be visualized from the orbit (II.g) through the optic chiasm (II.b).

compression by masses, such as pituitary macroadenoma, meningioma, or craniopharyngioma. The location of CN II.c in relation to the mass (**Fig. 4**) is of critical importance for procedural planning and is often clarified with the use of high-resolution imaging, such as CISS or fast imaging employing steady-state acquisition.<sup>21</sup> Intrinsic masses of the nerve, such as optic nerve gliomas, are most

commonly encountered in the pediatric population. Because the entirety of CN II is within the CNS, no Schwann cells exist to give rise to schwannomas.

#### CN II.d (Dural Cave): Anatomy

The definition of the dural cave segment of CN II is somewhat arbitrary, but it does exist and may

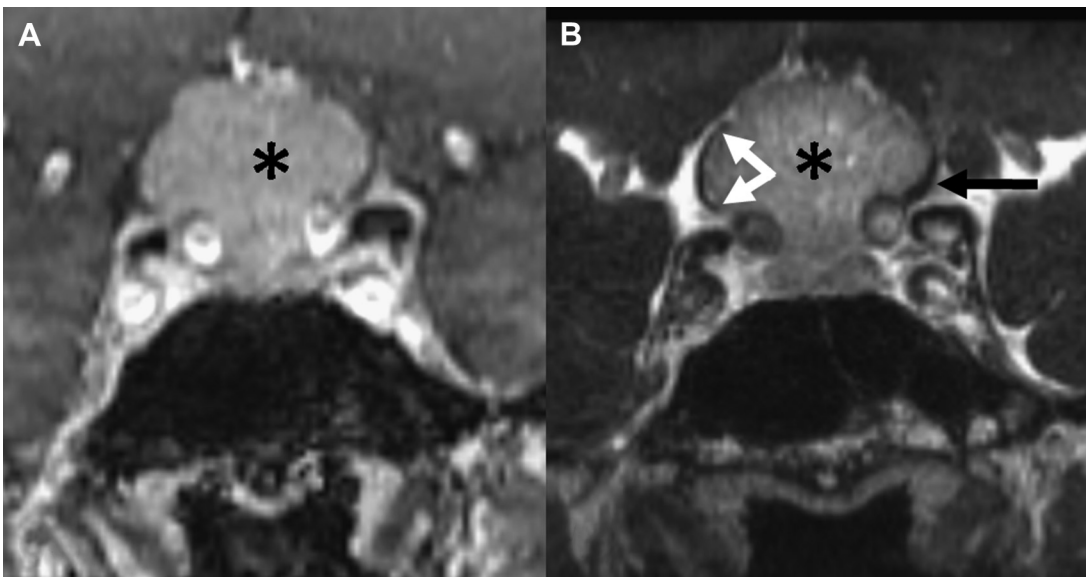


**Fig. 4.** (A) Postcontrast coronal T1 imaging demonstrates an enhancing extra-axial mass (*asterisk*) extending from the planum sphenoidale into the suprasellar cistern. (B) The relationship of the mass to the right CN II.c (*white arrows*) as well as the left CN II.c (*black arrow*) is best appreciated on postcontrast CISS. On postcontrast CISS, the mass extended along and deformed the CN II.d and proximal CN II.f segments while compressing the optic chiasm (CN II.b) (not shown). Meningioma was proven pathologically after debulking.

be seen as a CSF-filled recess partially surrounding the optic nerve before it emerges from the optic canal. The anterior border of CN II.d is difficult to define anatomically but may be construed on MR imaging as the point beyond which no CSF signal is visible. The posterior border of CN II.d is at the posterior margin of the anterior clinoid process.

### **CN II.f (Foraminal): Anatomy**

The optic nerves pass through the skull base via the optic canals (see **Fig. 3**), which are bounded by the anterior clinoid processes laterally and the orbital plates of the ethmoid bones medially. CN II.f may at times be difficult to evaluate on CISS because of susceptibility artifacts created by bone and air in the adjacent paranasal sinuses and sometimes pneumatized anterior clinoid process.

### **CN II.f: Selected Pathologic Conditions**

Masses in this region are often small and comparatively difficult to visualize. Meningioma is the most common mass lesion affecting CN II.f. Primary and secondary bony processes involving the anterior clinoid process and inflammatory and neoplastic processes involving the paranasal sinuses may also secondarily affect CN II.f.

### **CN II.g (Extraforaminal): Anatomy**

The optic nerve is visible within the orbit (see **Fig. 3B**) and is separated from the orbital fat by the optic nerve sheath, which contains fluid similar to CSF and variably communicates with the subarachnoid space.<sup>22</sup>

### **CN II.g: Selected Pathologic Conditions**

A myriad of neoplastic and non-neoplastic mass lesions may affect CN II.g. In case of intraorbital masses associated with the CN II.g, it is crucial for differential diagnosis and surgical planning to know whether the mass is originating from the optic nerve itself, the optic nerve sheath, or surrounding structures; whether the optic nerve is encased or displaced by tumor; and what the relative position of the nerve is compared with the mass. Postcontrast CISS imaging is often helpful in this regard because it shows the nerve against the enhancing tumor. Because the fat signal is not suppressed in CISS, the addition of high-resolution, postcontrast, fat-suppressed, T1-weighted images can be helpful in demonstrating enhancing tumor/orbital fat interface.

## **CN III: OCULOMOTOR NERVE**

The oculomotor nerve has both a motor function, innervating most of the muscles associated with the orbit, as well as a parasympathetic component that functions to constrict the pupil. The nuclei of the oculomotor nerve are located in the dorsal aspect of the midbrain just ventral to the cerebral aqueduct at the midline. From the nuclei, fibers course anteriorly and slightly laterally to exit the ventral aspect of the brainstem.

### **CN III.c (Cisternal Course): Anatomy**

The oculomotor nerve arises at the ventral aspect of the midbrain in the interpeduncular cistern. Within the cisternal segment, the oculomotor nerves course anteriorly and laterally in the interpeduncular cistern. The nerve passes between the posterior cerebral artery (PCA) superiorly and the superiorly cerebellar artery (SCA) inferiorly (**Fig. 5A**). The nerve then passes medial to the uncus of the temporal lobes (see **Fig. 5B**). The TZ of CN III.c is located, on average, approximately 1.9 mm from the apparent origin (range 1.0–4.0 mm).<sup>23</sup>

### **CN III.c: Selected Pathologic Conditions**

As the parasympathetic fibers of the nerve pass within its periphery, uncal herniation with CN III.c impingement will result in pupillary dilation caused by unopposed action of the sympathetic nervous system. Additionally, herniation of the uncus medially across the free edge of the tentorium may impinge on the nerve. Oculomotor palsy may result from compression of CN III.c by tumors or neurovascular compression, with findings on CISS correlating well with those at surgery.<sup>24</sup> Isolated reversible enhancement and thickening of CN III.c has been reported in ophthalmoplegic migraine by standard imaging<sup>25</sup>; one recent review of ophthalmoplegic migraine found that nerve thickening and enhancement is seen in 75% of cases diagnosed clinically.<sup>26</sup>

### **CN III.d (Dural Cave): Anatomy**

The dural cave of the CN III is a segment of variable length and is given the name of the oculomotor cistern. The length of the oculomotor cistern is reported on anatomic studies as ranging from 3.0 to 11.0 mm, averaging 6.5 mm,<sup>27</sup> and on MR imaging averaging 4.2 mm with a range of  $\pm 3.2$  mm, visualized in 75% of screening MR imaging with CISS.<sup>28</sup> CN III.d (see **Fig. 5**; **Fig. 6A**) extends from the oculomotor porus at the posterior margin of the oculomotor cistern to exit anteriorly into the lateral wall of the cavernous sinus at its superior extent (see **Fig. 6B**).

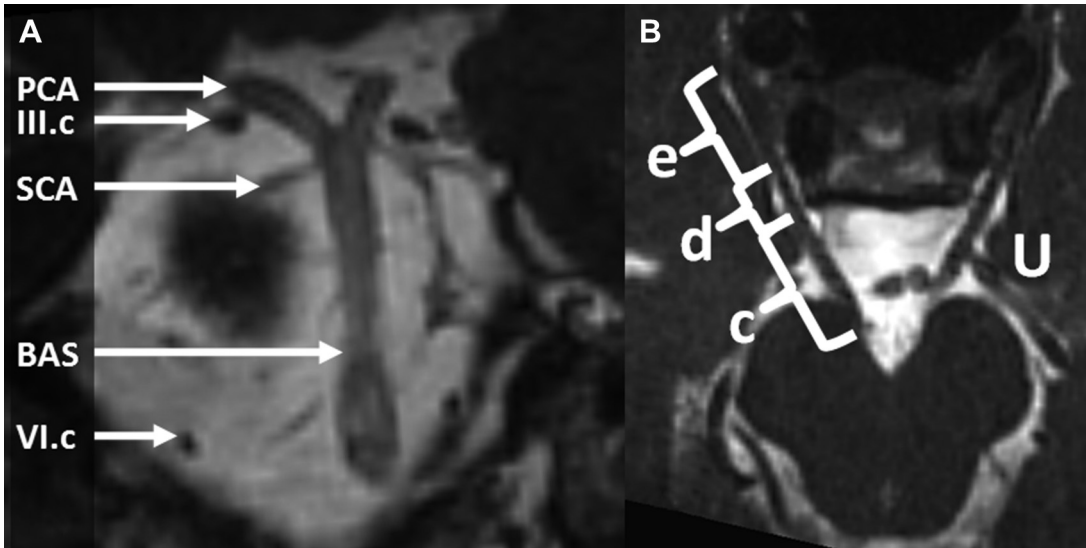


**Fig. 5.** (A) Coronal contrast-enhanced CISS demonstrates CN III.c (c) passing below the proximal PCA and above the SCA. The basilar artery (BAS) is also shown. (B) Axial oblique reformatted CISS with contrast demonstrating CN III.c as it arises from the midbrain within the interpeduncular cistern. The nerve extends anterolaterally coursing medial to the uncus (U). The CN III.d (d) segment is visible before the nerve pierces the dura to enter the cavernous sinus as CN III.e (e).

### ***CN III.e (Interdural): Anatomy***

CN III.e is entirely contained within the lateral wall of the cavernous sinus, with CN III entering the posterior aspect lateral to the posterior clinoid process and exiting the anterior aspect into the superior orbital fissure below the anterior clinoid process.<sup>29</sup> CN III.e is the most superior of the CNs within the cavernous sinus.

### ***CN III.e: Selected Pathologic Conditions***

Because the CN III.e is the most superior of the intracavernous cranial nerves, compressive lesions expanding from above, such as aneurysms arising from the posterior communicating artery (PCOM) origin or superior hypophyseal aneurysms, may lead to compression in this region (**Fig. 7**).

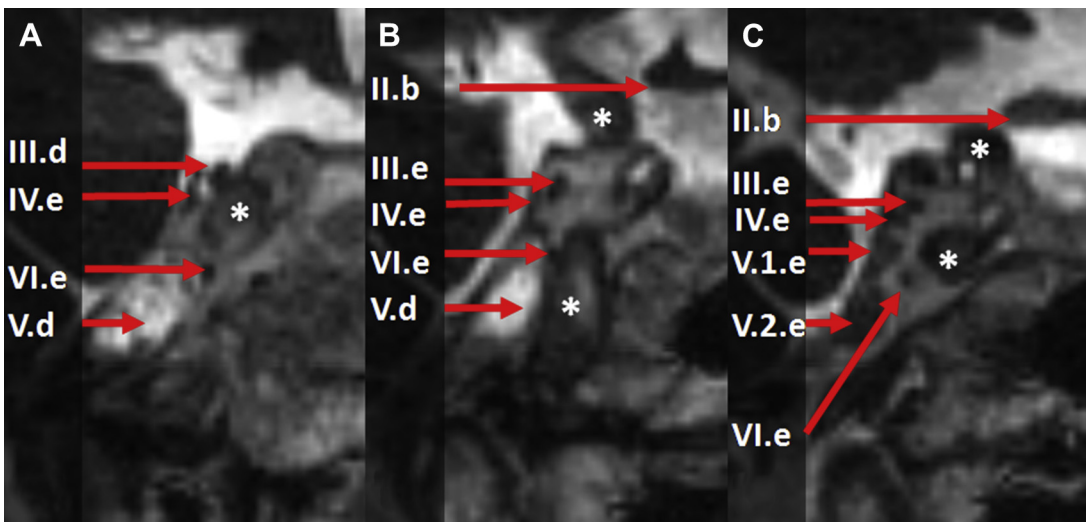


**Fig. 6.** Coronal postcontrast CISS through the cavernous sinus from posterior (A) to anterior (C). Cranial nerve segments as noted. The internal carotid artery is marked with an asterisk.

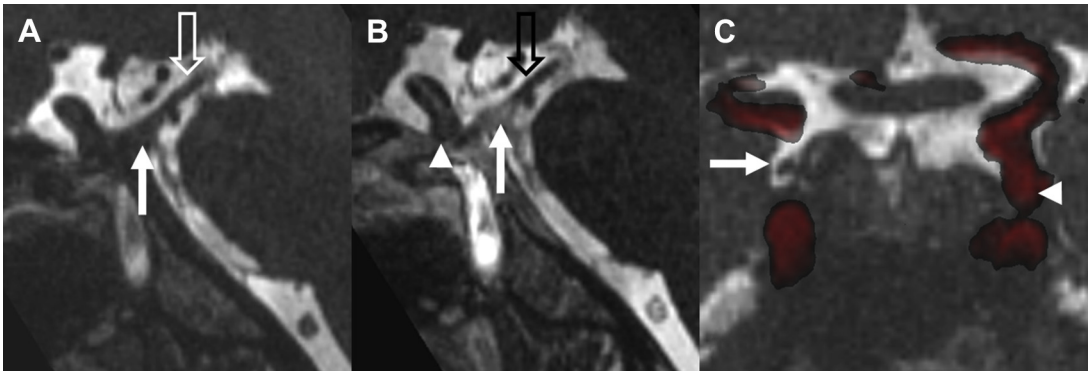


**Fig. 7.** A 38-year-old woman with left third nerve palsy. (A) Sagittal noncontrast CISS demonstrates a normal caliber of the midcisternal left CN III.c (*open arrow*) passing anteriorly between the PCA superiorly and the SCA inferiorly. The distal CN III.c is significantly thickened (*closed arrow*). (B) On the corresponding postcontrast CISS image, enhancement of the distal left CN III.c is seen (*closed arrow*) and the dome of a large PCOM origin aneurysm can be seen (*arrowhead*) overlying the cavernous sinus. (C) Coronal color-mapped fused time-of-flight MR angiography precontrast CISS demonstrates a normal right CN III.d (*arrow*) with the region of the corresponding left CN III.d/proximal CN III.e obliterated by the aneurysmal dome (*arrowhead*).

### CN III.f (Foraminal): Anatomy

CN III enters the superior orbital fissure from the superior aspect of the cavernous sinus where it courses superiorly.<sup>23,30</sup> As the oculomotor nerve passes anteriorly in the superior orbital fissure, it assumes an inferior position<sup>31</sup> within the central sector.<sup>32</sup> The nerve can be seen as a distinct structure at the posterior margin of the superior orbital fissure/anterior cavernous sinus (**Fig. 8**), although as the space narrows toward the orbital apex, typically, individual nerves are difficult to distinguish.

### CN III.g (Extraforaminal): Anatomy

On exiting from the superior orbital fissure, CN III.g passes anteriorly through the annulus of Zinn into the intraconal compartment of the orbit. The nerve then divides into a superior and inferior division. The superior division innervates the superior rectus muscle and continues medial to the superior rectus to innervate the levator palpebrae superioris muscle. The inferior division travels below the optic nerve and divides to innervate the inferior and medial recti as well as the inferior oblique

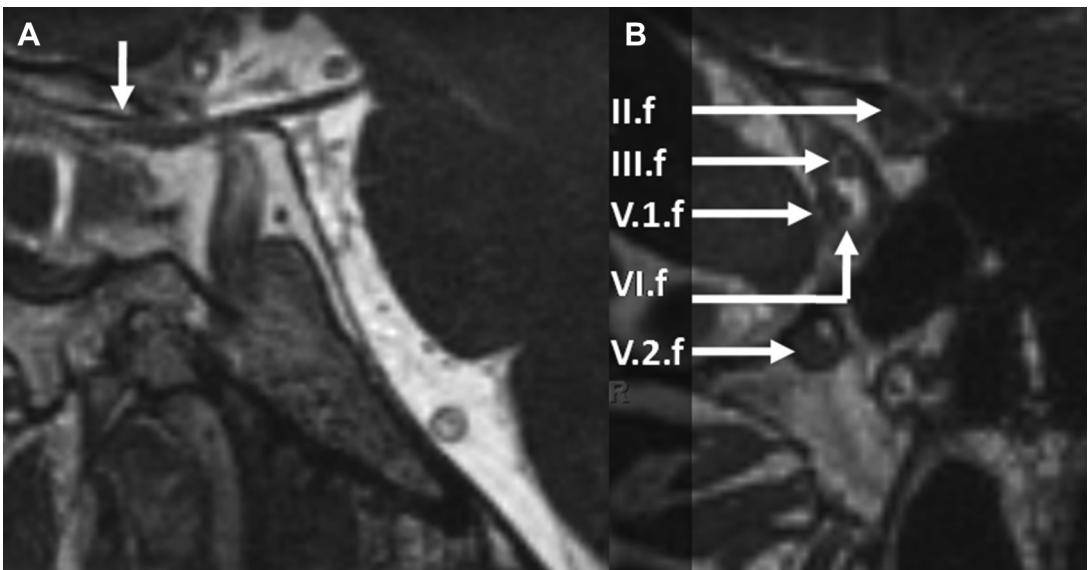


**Fig. 8.** (A) Sagittal postcontrast CISS demonstrates CN III extending from the brainstem anteriorly toward the superior orbital fissure (*arrow*). (B) Coronal postcontrast CISS through the level of the posterior aspect of the superior orbital fissure and optic canal.

and also carries parasympathetic fibers to the ciliary ganglion. The distal CN III.g branches destined for the extraocular muscles innervate their targets at the junction along the inner aspect of the muscle at the division between the posterior one-third and anterior two-thirds.<sup>33</sup>

### **CN III.g: Selected Pathologic Conditions**

(Fig. 9).

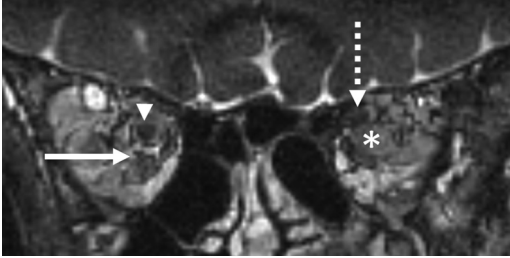


**Fig. 9.** A 42-year-old woman with atypical neurofibromatosis was initially diagnosed with a lesion of the left optic nerve at the orbital apex at an outside institution. Coronal postcontrast CISS on a 1.5-T magnet demonstrates a normal right CN III.g (arrowhead). The inferior division of the right CN III.g is also seen (arrow). On the left, an enhancing mass (asterisk) displaces the left CN II.g (dashed arrow) superiorly rather than arising from it and was thought to likely reflect a neurofibroma of the left inferior division of CN III.g.

### **CN IV: TROCHLEAR NERVE**

The trochlear nerve (CN IV) has the smallest diameter of the upper cranial nerves and innervates the superior oblique muscle. The nucleus of CN IV can be found in the caudal and dorsal midbrain and is exceptional in its location on the contralateral side of the brainstem from the muscle it innervates. The trochlear nerve is also unusual because it is the only cranial nerve to emerge from the dorsal aspect of the brainstem.

#### **CN IV.c (Cisternal): Anatomy**

The trochlear nerve emerges from the dorsal aspect of the caudal midbrain just below the inferior colliculi and on either side of the frenulum of the superior medullary velum<sup>34</sup> within the quadrigeminal cistern (Fig. 10) and courses laterally and then anteriorly into the ambient cistern along the lateral aspect of the midbrain.<sup>35</sup> Yousry and colleagues<sup>36</sup> found that the apparent origin varied from 3 to 9 mm from the midline on CISS imaging. Because of its small size, even the proximal cisternal segment is not always routinely visualized; however,

Choi and colleagues,<sup>37</sup> using 3D-balanced turbo-field echo (bTFTE) in healthy research subjects undergoing acquisitions lasting in excess of 7 minutes, have reported that with voxels smaller than the nerve diameter, CN IV.c may be visualized 100% of the time. The investigators suggest with sufficient spatial resolution, the nerve could be differentiated from the small adjacent vasculature structures that might otherwise be mistakenly identified as the nerve itself and measured a mean diameter of 0.54 mm (range 0.35–0.96 mm).<sup>37</sup> In its distal component, CN IV.c passes under the free edge of the tentorium cerebelli where it is potentially vulnerable during operative approaches to this region<sup>38</sup> and is not typically well visualized on imaging.<sup>36</sup> Although CN IV.c is seen as a single root when it is visualized on MR imaging, 2 rootlets may arise from the brainstem on anatomic studies; this was seen 31% of the time in one study with the rootlets arising up to 4 mm apart.<sup>39</sup> Given the small size and consequent challenge of visualization of even a solitary root of the CN IV.c, it is possible that such variant anatomy could partly account for the significant variation in diameter and detection of the trochlear nerve reported on imaging. The TZ is located, on average, 0.3 mm from the apparent origin (range 0–1.0 mm).<sup>23</sup>

#### **CN IV.c: Selected Pathologic Conditions**

As with the other CNs (except CN I and II), peripheral nerve sheath tumors may arise from CN IV.c. In addition, CN IV.c passes just below the tentorium cerebelli and may be compressed by masses in this region. Fig. 10 demonstrates a small mass arising from the left CN IV.c or adjacent tentorium in a patient presenting with left superior oblique palsy. Myokymia of the superior oblique caused by neurovascular conflict has been reported.<sup>36</sup> Congenital absence of the fourth cranial nerve has been demonstrated via lack of visualization of CN IV.c in congenital superior oblique palsy with superior oblique hypoplasia with voxel size of 0.3 × 0.3 × 0.25 mm.<sup>40</sup>

#### **CN IV.d (Dural Cave)**

CN IV is not typically associated with a visible dural cave. The nerve pierces the lamina propria of the dura caudal to the intersection of the free and attached segments of the tentorium cerebelli.<sup>38</sup>

#### **CN IV.e (Interdural)**

The interdural course of CN IV is entirely contained within the lateral wall of the cavernous sinus, entering posterolateral to CN III.e.<sup>29</sup>

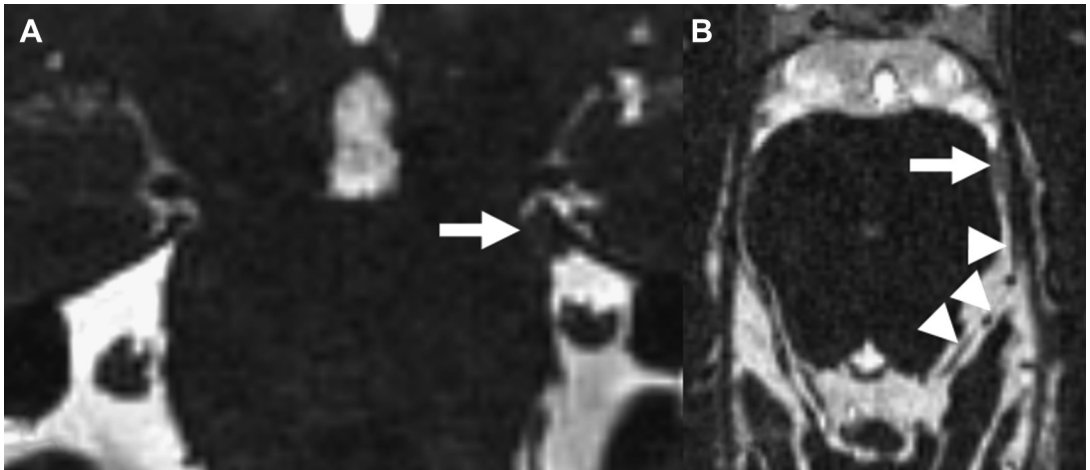


**Fig. 10.** A 38-year-old woman presenting with a left CN IV palsy. (A) Coronal CISS without contrast demonstrates an asymmetric filling defect within the subarachnoid space (*arrow*) caused by a mass measuring up to 5 mm along the undersurface of the free edge of left aspect of the tentorium cerebelli. (B) On postcontrast CISS in the axial plane (3T, 0.5 mm isotropic resolution), the left CN IV.c (*arrowheads*) can be seen extending through the ambient cistern into the region of the mass, which demonstrates enhancement (*arrow*).

### **CN IV.f (Foraminal)**

CN IV.f passes through the superior aspect of the superior orbital fissure<sup>31</sup> in the lateral sector<sup>32</sup> and is hard to detect in this region.

### **CN IV.g (Extraforaminal)**

CN IV.g enters the orbit superior to the annulus of Zinn and runs below the orbital roof to innervate the superior oblique muscle joining the muscle within the posterior third.<sup>33</sup>

## **CN V: TRIGEMINAL NERVE**

The trigeminal nerve (CN V) has the largest diameter of the CNs and serves sensation from the face with its three main segments (V.1 [ophthalmic], V.2 [maxillary], V.3 [mandibular]) (**Fig. 11**) as well as innervates the muscles of mastication through the V.3 segment. The nuclei and tracts of the trigeminal nerve are extensive, ranging from the midbrain through the upper cervical spinal cord.

### **CN V.c (Cisternal): Anatomy**

The apparent origin of the trigeminal nerve is at the lateral aspect of the belly of the pons. The motor roots may arise separately from the main mass of the nerve and are typically seen as separate structures arising superiorly and medially. When seen separately, there may be between 1 and 3 motor roots.<sup>41</sup> The TZ of the sensory root of CN V.c is variously reported as extending, on average, approximately 3.6 mm from the apparent origin

(range 2.0–6.0 mm)<sup>23</sup> to 4.2 mm from the apparent origin (range 3.4–5 mm)<sup>42</sup> for the sensory root. For the motor roots, TZ is located, on average, 0.3 mm from the apparent origin (range 0–1.0 mm).<sup>23</sup>

### **CN V.c: Selected Pathologic Conditions**

Facial pain caused by an abnormality of the trigeminal nerve, trigeminal neuralgia (TGN, also known as tic douloureux), is a particularly vexing clinical problem. When pain is associated with analgesia in the sensory distribution of the trigeminal nerve or one of its main 3 components, a mass is often suspected. In the absence of a mass, suspicion falls on the possibility of neurovascular compression (**Fig. 12**). The relationship of vascular structures within the cistern to CN V.c is often accurately depicted with CISS, although some investigators have not found predictions on high-resolution imaging to be entirely reliable.<sup>43</sup> Additionally, the finding of neurovascular compression is not uncommon in the asymptomatic population or on the asymptomatic side<sup>44</sup>; the surgical decision of microvascular decompression in patients with TGN should be made by the combination of clinical and radiological findings. The measurement of diameter and cross-sectional area on CISS has been reported to demonstrate decreased size of the CN V.c on the symptomatic side.<sup>45</sup> The combination of high-spatial-resolution imaging with DTI may allow for higher specificity for TGN<sup>46</sup> with substantially decreased FA associated with neurovascular compression.

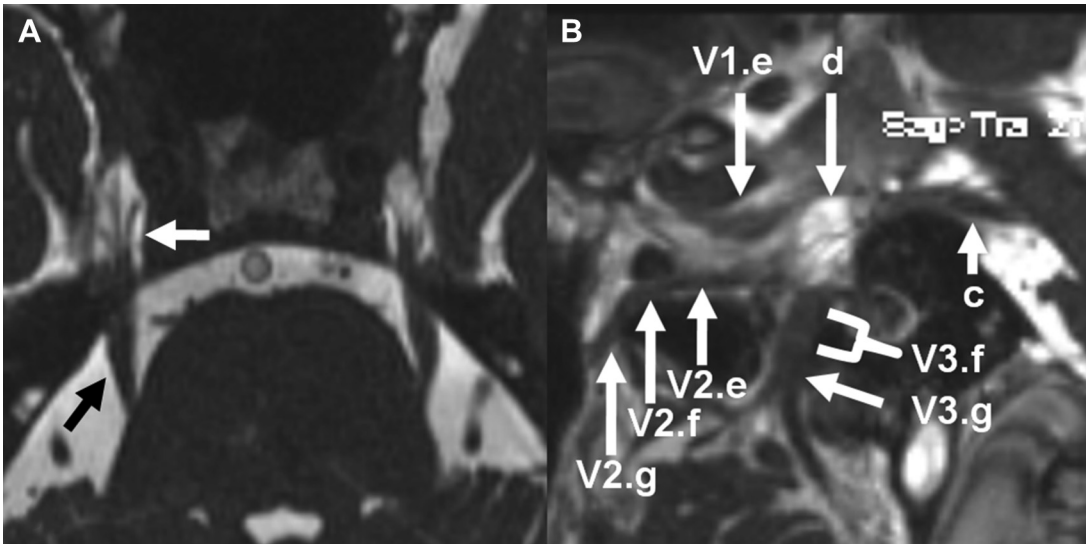


**Fig. 11.** (A) Axial noncontrast CISS demonstrates CN V.c emerging from the lateral pons (*black arrow*) extending through the porus trigeminus into the Meckel cave (*white arrow*) where fibers of CN V.d can be seen. (B) On sagittal oblique postcontrast CISS, CN V.c roots can be seen entering the Meckel cave (d) through the trigeminal porus with individual CN V.d fibers noted surrounded by CSF. CN V.1.e and CN V.2.e are seen extending anteriorly through the cavernous sinus. V.2.f continues through foramen rotundum into the pterygopalatine fossa as V.2.g. V.3.f extends caudally through foramen ovale with proximal branching of V.3.g visible in this image.

### CN V.d: (Dural Cave) Anatomy

The dural cave of CN V is the most constant of all of the cranial nerves and is called Meckel cave (also known as the trigeminal cistern). The gasserian (also known as the semilunar or trigeminal) ganglion, which sits along the floor and anterior wall, is well visualized with contrast-enhanced

CISS.<sup>47</sup> Distal to the gasserian ganglion, the nerve divides into 3 divisions: V1 (ophthalmic), V2 (maxillary), and V3 (mandibular) (see **Fig. 11B**).

### CN V.1.e (Interdural)

CN V.1.e, the interdural component of the ophthalmic division of the trigeminal nerve, enters

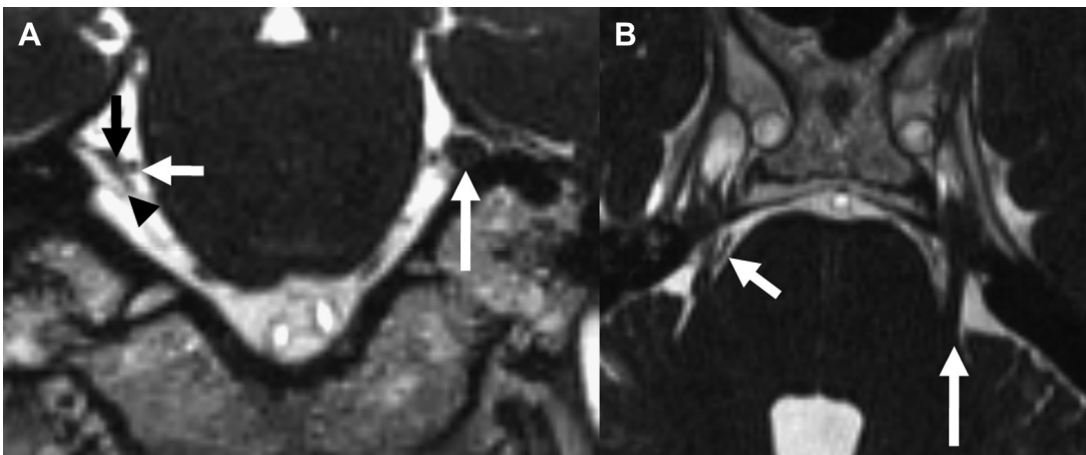


**Fig. 12.** A 52-year-old man with right-sided TGN. (A) Coronal reformatted postcontrast CISS demonstrates compression of the right CN V.c (*black arrow*) by a branch of the right superior cerebellar artery medially (*short white arrow*) and an enhancing venous structure (*black arrowhead*) coursing along its inferior and lateral aspect. The cross-sectional area of the right CN V.c is reduced when compared with the contralateral unaffected side (*long white arrow*). (B) On axial reformatted images, the right superior cerebellar artery (*short arrow*) can be seen traversing the superior margin of the right CN V.c. The left CN V.c (*long arrow*) is unimpinged.

the lower portion of the lateral wall of the cavernous sinus (see **Fig. 6C**) and extends anteriorly and superiorly (see **Fig. 11B**) toward the superior orbital fissure.<sup>29</sup> Dissections have demonstrated that the sympathetic fibers that extend from the adventitia of the internal carotid artery typically travel briefly with CN VI.e before joining CN V.1.e in this region.<sup>48</sup>

### **CN V.1.f (Foraminal)**

At the anterior aspect of the cavernous sinus/posterior aspect of the superior orbital fissure, CN V.1.f is located laterally before final branching (see **Fig. 8B**). The frontal and lacrimal branches of V.1 pass anteriorly through the superior aspect of the superior orbital fissure, whereas the nasociliary branch of V.1 passes through the inferior aspect of the superior orbital fissure.<sup>31</sup>

### **CN V.1.g (Extraforaminal)**

The frontal branch extends through the supraorbital foramen to supply sensation to the upper face. The lacrimal branch supplies sensation to the lacrimal gland. The nasociliary branch of V.1, through long and short ciliary branches, innervates the globe and is responsible for the afferent input for the corneal reflex with additional branches extending into the nasal cavity.

### **CN V.2.e (Interdural)**

CN V.2.e, the interdural component of the maxillary division of the trigeminal nerve, enters the cavernous sinus just below CN V.1.e (see **Fig. 6C**).

### **CN V.2.f (Foraminal)**

The V.2.f passes anteriorly through the foramen rotundum (see **Fig. 8B**) where it is surrounded by a perineural vascular plexus<sup>49</sup> and is well visualized on contrast-enhanced CISS.<sup>47</sup>

### **CN V.2.g (Extraforaminal)**

V.2 emerges from the foraminal segment into the pterygopalatine fossa where CN V.2.g divides into 3 main branches: the infraorbital nerves, which travel anteriorly through the infraorbital foramen to provide sensation to the midportion of the face; the zygomatic nerve, which extends through the inferior orbital fissure to supply the lacrimal gland; and the superior alveolar nerves, which provide sensation to the maxillary teeth.<sup>50</sup>

### **CN V.3.e (Interdural)**

The V.3.e segment is quite short because the nerve passes inferiorly from the Meckel cave.

### **CN V.3.f (Foraminal)**

The V.3 segment passes inferiorly and laterally through the foramen ovale where it is surrounded by a perineural vascular plexus<sup>49</sup> and is well visualized on contrast-enhanced CISS<sup>47</sup> (see **Fig. 12B**).

### **CN V.3.g (Extraforaminal)**

CN V.3.g passes inferiorly into the masticator space. Multiple branch points of CN V.3.g are routinely visualized in the authors' experience (see **Fig. 12B**). Termination of distal branches in the muscles of mastication, which they innervate, is often visible. Sensory branches are also seen; the inferior alveolar nerve, for instance, can be followed to the mandibular foramen in most cases.

## **CN VI: ABDUCENS NERVE**

The abducens nerve (also spelled *abducent*) has a single motor function: innervation of the lateral rectus muscle. The nucleus of the abducens nerve lies in the dorsal medial aspect of the caudal pons with fibers forming a tract and the fascicular segment extending anterolaterally toward the pontomedullary junction ventrally.

### **CN VI.c (Cisternal): Anatomy**

The apparent origin of CN VI.c is typically found at the pontomedullary junction, although rootlets may arise from the caudal pons in approximately 18% of anatomic specimens.<sup>51</sup> The nerve extends superiorly within the prepontine cistern (see **Figs. 13** and **5A**); although visualization was initially limited to 79% with 1-mm sections,<sup>52</sup> CN VI.c is now well seen on CISS imaging, identifiable in nearly all cases.<sup>53</sup> Anatomic studies suggest that CN VI.c may arise as one or multiple rootlets<sup>51</sup> and, if the nerve arises as one root, may split into 2 roots within its cisternal course. Adjacent vascular structures may abut, encircle, or divide single roots or multiple rootlets.<sup>51</sup> A single nerve along the entirety of the course is most common, reported in approximately 87%<sup>54</sup> to 92%<sup>55</sup> of anatomic specimens. One study with 3D turbo spin echo reported 2 CN VI.c rootlets unilaterally in approximately 20% of individuals and bilateral double rootlets in approximately 5% of patients,<sup>56</sup> although it is not clear how the investigators excluded the possibility that some of the cases reflected vascular structures in the area studied, a factor that can lead to misidentification of cisternal segments of the cranial nerves in other contexts.<sup>37</sup> The TZ is located on average 0.3 mm from the apparent origin (range 0–1.0 mm).<sup>23</sup>

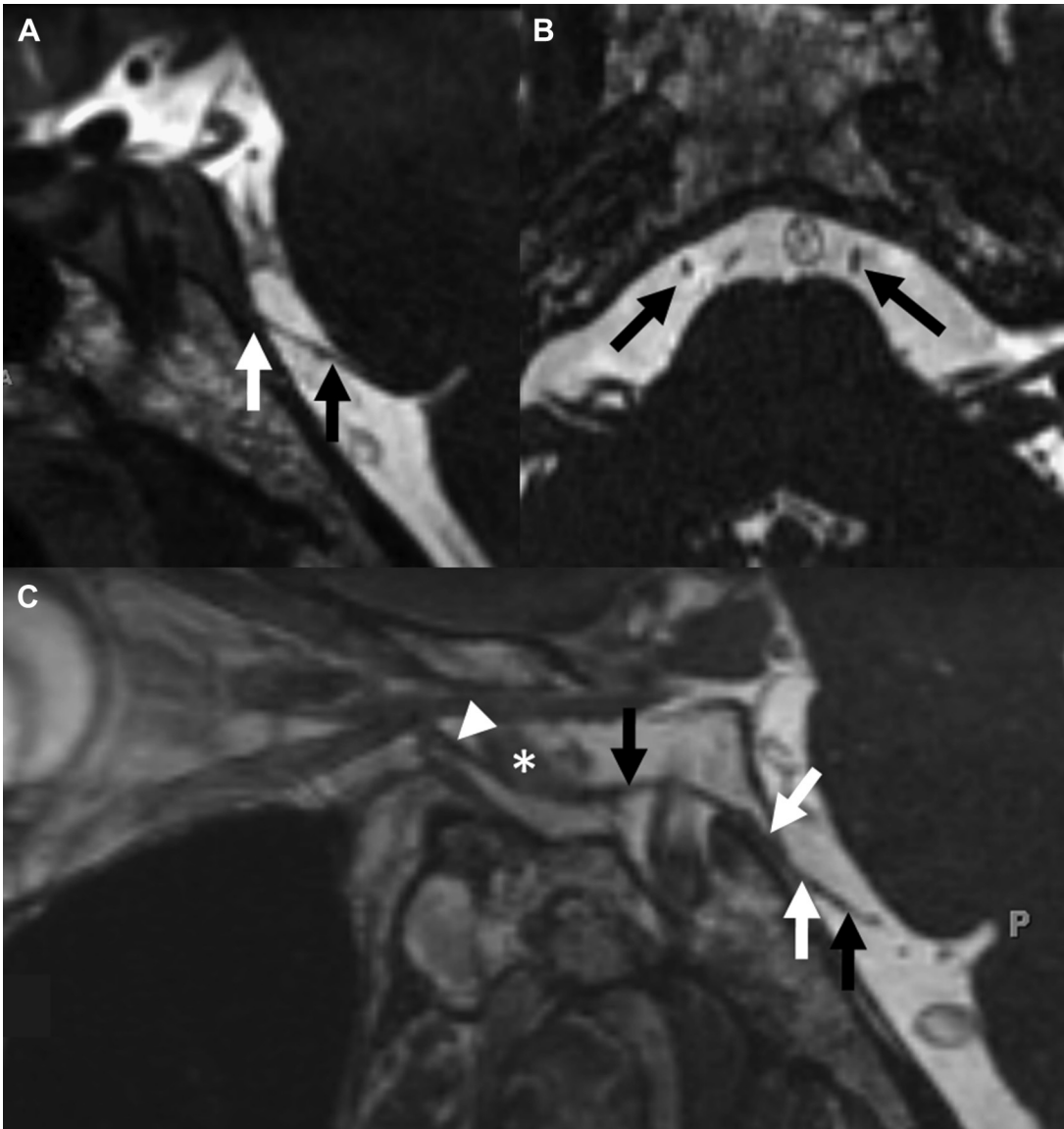


**Fig. 13.** (A) Sagittal oblique CISS without contrast demonstrates VI.c (black arrow) emerging from the pontomedullary junction and extending superiorly and anteriorly toward the dorsal clivus. CN VI.d is shallow in this case, without significant evagination of CSF (white arrow). (B) Axial CISS demonstrates both CN.c segments at the mid-cisternal component (arrows). (C) Postcontrast sagittal oblique CISS demonstrates CN VI.c (black upward arrow) extending to pierce the inner layer of dura without a significant CN VI.d segment (white upward arrow). CN VI.e extends through the petroclival (white downward arrow) into the cavernous segment (black downward arrow), passing adjacent to the cavernous internal carotid artery (asterisk) to enter the superior orbital fissure as CN VI.f (arrowhead).

### CN VI.c: Selected Pathologic Conditions

The abducens nerve may be congenitally absent, a fact that is most easily verified in the cisternal segment.<sup>57,58</sup>

### CN VI.d (Dural Cave): Anatomy

The dural cave segment of CN VI is defined on an imaging basis by visualization of CSF surrounding

the nerve (Fig. 14A). The length of CN VI.c is variable, with corresponding variability on the position of CN VI.d. Additionally, the CN VI.d segment is variable in length and may be extremely short in some cases; however, imaging studies demonstrate that this segment measured 1 mm or greater in length approximately 57%<sup>53</sup> to 86% of the time.<sup>59</sup> Despite the apparently relatively diminutive length of this segment on imaging, the arachnoid

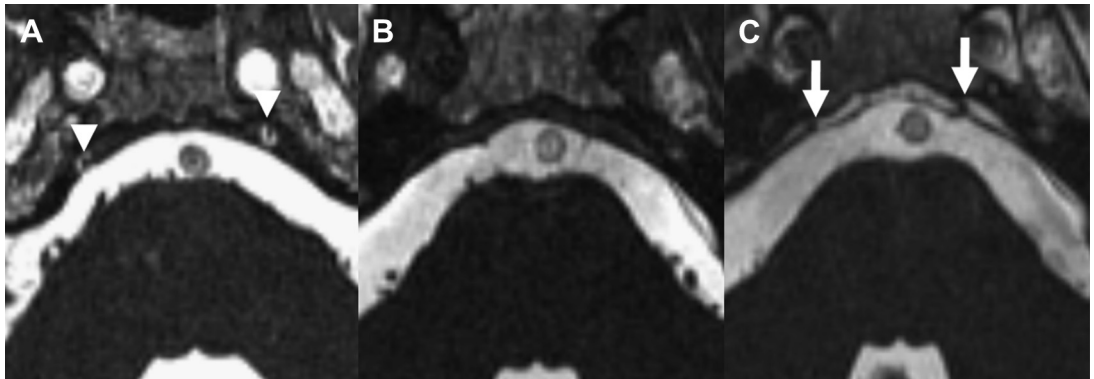


**Fig. 14.** (A) Axial precontrast CISS imaging through the level of the midpons in a patient with prominent bilateral dural caves. CN VI.d (arrowheads) is well visualized surrounded by CSF. (B) In other patients without a significant dural cave segment, CN VI.e is not well visualized at the same level before contrast administration, having passed through the junction of the CSF with the inner layer of dura. Note opacification of the petroclival venous confluence once intravenous contrast is administered (C) opacification of surrounding venous structures allows for visualization of the bilateral petroclival CN VI.e segments (arrows).

membrane may follow the nerve throughout the petroclival segment to the level of the petrosphenoidal ligament,<sup>60</sup> presumably creating a potential space. Anatomic studies suggest that when multiple CN VI.c roots are present, they pierce the inner layer of dura separately,<sup>54</sup> presumably with the potential for focal evagination of the CSF at each point of contact with the dura. For the purposes of imaging classification, CN VI.d is designated as the portion of the nerve surrounded by visible fluid within an evagination in communication with the subarachnoid space.

### **CN VI.e (Interdural): Anatomy**

The segment of the abducens nerve is the longest of the cranial nerves and is itself divided into 2 subsegments. The proximal segment has been termed the *gulfar component* by Iaconetta and colleagues,<sup>55</sup> although in practice this term is not commonly used and the authors prefer the term *petroclival segment* as used by Yousry and colleagues,<sup>53</sup> Joo and colleagues,<sup>61</sup> and Umansky and colleagues.<sup>62</sup> CN VI.e extends superiorly through the inferior petrosal sinus (when individually defined and bilateral) or petroclival venous confluence<sup>55</sup> (when a venous plexus is present) into the Dorello canal typically coursing under the petrosphenoidal (Gruber) ligament before entering the cavernous segment. The usage of the term *Dorello canal* itself is somewhat confusing because it has sometimes been applied in the radiology literature<sup>52</sup> to the entirety of the petroclival segment, possibly in some instances including the dural cave segment.<sup>52,53</sup> Several investigators suggest that it should be properly reserved solely for the point at which the nerve passes under the the

petrosphenoidal ligament.<sup>60,62</sup> For the purposes of this article, the authors use the term *Dorello canal* in the more narrow sense as that point of transition between the petroclival and cavernous interdural subsegments of CN VI.e, where the nerve passes under the Gruber ligament,<sup>63</sup> changing its course to extend anteriorly into the cavernous sinus.

### **CN VI.e: Petroclival Subsegment**

The petroclival portion of CN VI.e courses over the dorsal aspect of the clivus between the inner and outer layers of dura surrounded by a variably robust network of venous channels, the confluent portion of which over the rostral clivus has been termed the *petroclival venous confluence*.<sup>64</sup> Just as the CN VI.d/CN VI.e junction is variable in position, the CN VI.d/CN VI.e junction is correspondingly variable. When a relatively inferior entrance of the nerve into the interdural space is observed, CN VI.e may be seen as it extends superiorly surrounded by venous blood of the inferior petrosal sinus<sup>61</sup> coursing superiorly into the petroclival venous confluence. In some cases, particularly those with a more superior entrance to the dura, the proximal petroclival segment may begin surrounded by the petroclival venous confluence. Anatomic studies suggest that when 2 roots are present, one will depart the dorsal clival segment above and the other below the Gruber ligament.<sup>54</sup> On imaging, the distinction between CN VI.d and the petroclival CN VI.e is made by visualization of the presence of surrounding CSF; however, on anatomic studies, the arachnoid membrane<sup>60</sup> and an accompanying dural sleeve<sup>61</sup> actually follow the nerve as far

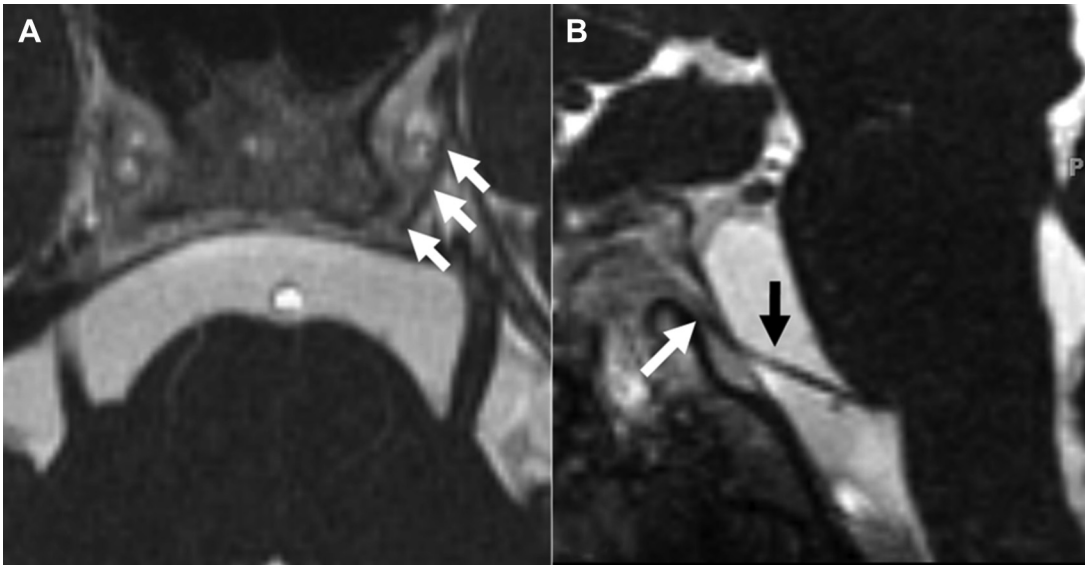


**Fig. 15.** Several-day history of abducens palsy on the right. Standard protocol MR imaging unremarkable. Post-contrast isotropic CISS. (A) Axial image. The left CN VI.e (arrows) is well visualized extending through Dorello canal into the cavernous sinus. The right abducens nerve is not visualized in the cavernous region because of pathologic enhancement. (B) In sagittal oblique reformatted views, CN VI.c (black arrow) and the proximal CN VI.e segment are seen with an abrupt transition to the region of pathologic enhancement (white arrow). Tolosa-Hunt syndrome was suggested. No significant CN VI.d segment was present in this individual, a feature of significant variation between patients.

superiorly as the Gruber ligament. Regardless, from an imaging perspective, the nerve is not typically visible in this region without the aid of contrast enhancement in the surrounding venous blood (see Fig. 14).

### **CN VI.e: Cavernous Subsegment**

The cavernous segment of CN VI.e, alone among the CNs, traverses the main compartment of the cavernous sinus (rather than running in the fibrous lateral wall). The nerve can be found lateral to the cavernous carotid artery soon after it enters from the petroclival segment. Based on work with dissection, Harris and Rhoton<sup>65</sup> describe up to 5 roots of CN VI.e in this region, although in most cases only a single root was seen. In the authors' experience, CN VI.e may be obscured where it passes directly lateral to the cavernous internal carotid artery but is otherwise well seen in the cavernous interdural segment. The sympathetic nerves that ultimately innervate the orbit travel briefly with CN VI.e in this region before joining CN V.1.e.<sup>48,66</sup>

### **CN VI.e: Selected Pathologic Conditions**

**Fig. 15** demonstrates pathologic enhancement of CN VI.e, which was presumed to be caused

by inflammation, the so-called Tolosa-Hunt syndrome.

### **CN VI.f (Foraminal)**

CN VI.f passes through the inferior aspect of the superior orbital fissure<sup>31</sup> within its central sector.<sup>32</sup>

### **CN VI.g (Extraforaminal)**

The abducens nerve travels anteriorly along the medial aspect of the lateral rectus muscle to insert at the junction between the posterior one-third and anterior two-thirds of the muscle.<sup>33</sup>

## **SUMMARY**

This article reviews the high-resolution anatomy and appearance of the cisternal through proximal extraforaminal segments of CN I to CN VI, following the classification scheme proposed in the accompanying article by Blitz, Choudhri, Chonka and colleagues on the segmental anatomy of the cranial nerves and imaging techniques. The cisternal and dural cave segments of the upper cranial nerves, with the possible exception of the fourth cranial nerve, are well evaluated with noncontrast CISS. The interdural and foraminal segments of the CNs are revealed after the administration of intravenous contrast. The proximal extraforaminal segments of the

cranial nerves are also often well visualized on 3D high-resolution imaging with CISS. Evaluation for pathologic contrast enhancement is also now possible at a smaller scale and in regions of the upper cranial nerves which were previously not well seen.

## REFERENCES

- Casselmann J, Kuhweide R, Deimling M, et al. Constructive interference in steady state-3DFT MR imaging of the inner ear and cerebellopontine angle. *AJNR Am J Neuroradiol* 1993;14(1):47–57.
- Yagi A, Sato N, Taketomi A, et al. Normal cranial nerves in the cavernous sinuses: contrast-enhanced three-dimensional constructive interference in the steady state MR imaging. *AJNR Am J Neuroradiol* 2005;26(4):946–50.
- Shigematsu Y, Korogi Y, Hirai T, et al. Contrast-enhanced CISS MRI of vestibular schwannomas: phantom and clinical studies. *J Comput Assist Tomogr* 1999;23(2):224.
- Brazis PW, Masdeu JC, Biller J. *Localization in Clinical Neurology*. Philadelphia: Lippincott Williams & Wilkins; 2011.
- Naidich TP, Duvernoy HM, Delman BN, et al. *Duvernoy's Atlas of the Human Brain Stem and Cerebellum*. Vienna (Austria): Springer-Verlag; 2009.
- Nieuwenhuys R, Voogd J, Voogd J, et al. *The Human Central Nervous System*. New York: Springer Verlag; 2008.
- Doucette R. PNS-CNS transitional zone of the first cranial nerve. *J Comp Neurol* 1991;312(3):451–66.
- Yousry I, Camelio S, Schmid U, et al. Visualization of cranial nerves I–XII: value of 3D CISS and T2-weighted FSE sequences. *Eur Radiol* 2000;10(7):1061–7.
- Borges A, Casselman J. Imaging the cranial nerves: part I: methodology, infectious and inflammatory, traumatic and congenital lesions. *Eur Radiol* 2007;17(8):2112–25.
- Yousem DM, Geckle RJ, Bilker WB, et al. Olfactory bulb and tract and temporal lobe volumes: normative data across decades. *Ann N Y Acad Sci* 1998;855(1):546–55.
- Buschhüter D, Smitka M, Puschmann S, et al. Correlation between olfactory bulb volume and olfactory function. *Neuroimage* 2008;42(2):498–502.
- Abolmaali N, Gudziol V, Hummel T. Pathology of the olfactory nerve. *Neuroimaging Clin N Am* 2008;18(2):233–42.
- Laitinen EM, Vaaralahti K, Tommiska J, et al. Incidence, phenotypic features and molecular genetics of Kallmann syndrome in Finland. *Orphanet J Rare Dis* 2011;6(1):41.
- Rombaix P, Potier H, Markessis E, et al. Olfactory bulb volume and depth of olfactory sulcus in patients with idiopathic olfactory loss. *Eur Arch Otorhinolaryngol* 2010;267(10):1551–6.
- Haehner A, Hummel T, Hummel C, et al. Olfactory loss may be a first sign of idiopathic Parkinson's disease. *Mov Disord* 2007;22(6):839–42.
- Ponsen MM, Stoffers D, Twisk JW, et al. Hyposmia and executive dysfunction as predictors of future Parkinson's disease: a prospective study. *Mov Disord* 2009;24(7):1060–5.
- Koss E, Weiffenbach JM, Haxby JV, et al. Olfactory detection and identification performance are dissociated in early Alzheimer's disease. *Neurology* 1988;38(8):1228–32.
- Collet S, Grulois V, Bertrand B, et al. Post-traumatic olfactory dysfunction: a cohort study and update. *B-ENT* 2009;5(Suppl 13):97–107.
- Gallia GL, Reh DD, Salmasi V, et al. Endonasal endoscopic resection of esthesioneuroblastoma: the Johns Hopkins Hospital experience and review of the literature. *Neurosurg Rev* 2011;34:1–11.
- Becker M, Masterson K, Delavelle J, et al. Imaging of the optic nerve. *Eur J Radiol* 2010;74(2):299–313.
- Watanabe K, Kakeda S, Yamamoto J, et al. Delineation of optic nerves and chiasm in close proximity to large suprasellar tumors with contrast-enhanced FIESTA MR Imaging. *Radiology* 2012;264(3):852–8.
- Killer H, Jaggi G, Flammer J, et al. Cerebrospinal fluid dynamics between the intracranial and the subarachnoid space of the optic nerve. Is it always bidirectional? *Brain* 2007;130(2):514–20.
- Lang J. *Clinical Anatomy of the Head*. Berlin: Springer-Verlag; 1983.
- Sun X, Liang C, Liu C, et al. Oculomotor paralysis: 3D-CISS MR imaging with MPR in the evaluation of neuralgic manifestation and the adjacent structures. *Eur J Radiol* 2010;73(2):221–3.
- Mark AS, Casselman J, Brown D, et al. Ophthalmoplegic migraine: reversible enhancement and thickening of the cisternal segment of the oculomotor nerve on contrast-enhanced MR images. *AJNR Am J Neuroradiol* 1998;19(10):1887–91.
- Gelfand AA, Gelfand JM, Prabakhar P, et al. Ophthalmoplegic "migraine" or recurrent ophthalmoplegic cranial neuropathy: new cases and a systematic review. *J Child Neurol* 2012;27(6):759–66.
- Martins C, Yasuda A, Campero A, et al. Microsurgical anatomy of the oculomotor cistern. *Neurosurgery* 2006;58(4):ONS-220–7.
- Everton K, Rassner U, Osborn A, et al. The oculomotor cistern: anatomy and high-resolution imaging. *AJNR Am J Neuroradiol* 2008;29(7):1344–8.

29. Inoue T, Rhoton AL Jr, Theele D, et al. Surgical approaches to the cavernous sinus: a microsurgical study. *Neurosurgery* 1990;26(6):903.
30. Ettl A, Zwrtek K, Daxer A, et al. Anatomy of the orbital apex and cavernous sinus on high-resolution magnetic resonance images. *Surv Ophthalmol* 2000;44(4):303–23.
31. Morard M, Tcherekayev V, de Tribolet N. The superior orbital fissure: a microanatomical study. *Neurosurgery* 1994;35(6):1087–93.
32. Natori Y, Rhoton AL Jr. Microsurgical anatomy of the superior orbital fissure. *Neurosurgery* 1995;36(4):762–75.
33. Lemke BN, Lucarelli MJ. Anatomy of the ocular adnexa, orbit, and related facial structures. In: Black EH, Nesi FA, Gladstone GJ, et al, editors. *Smith and Nesi's Ophthalmic Plastic and Reconstructive Surgery*. New York: Springer; 2012. p. 3–58.
34. Netter F. *The Ciba Collection of Medical Illustrations, Volume 1: Nervous System; part 1: Anatomy and Physiology*. West Caldwell: CIBA Limited; 1983.
35. Rhoton AL Jr. The posterior fossa cisterns. *Neurosurgery* 2000;47(3):S287–97.
36. Yousry I, Moriggl B, Dieterich M, et al. MR anatomy of the proximal cisternal segment of the trochlear nerve: neurovascular relationships and landmarks<sup>1</sup>. *Radiology* 2002;223(1):31–8.
37. Choi B, Kim J, Jung C, et al. High-resolution 3D MR imaging of the trochlear nerve. *AJNR Am J Neuroradiol* 2010;31(6):1076–9.
38. Tubbs RS, Oakes WJ. Relationships of the cisternal segment of the trochlear nerve. *J Neurosurg* 1998;89(6):1015–9.
39. Bisaria K, Premsagar I, Lakhtakia P, et al. The superficial origin of the trochlear nerve with special reference to its vascular relations. *J Anat* 1990;170:199.
40. Kim JH, Hwang JM. Absence of the trochlear nerve in patients with superior oblique hypoplasia. *Ophthalmology* 2010;117(11):2208–13.
41. Yousry I, Moriggl B, Holtmannspoetter M, et al. Detailed anatomy of the motor and sensory roots of the trigeminal nerve and their neurovascular relationships: a magnetic resonance imaging study. *J Neurosurg* 2004;101(3):427–34.
42. Guclu B, Sindou M, Meyronet D, et al. Cranial nerve vascular compression syndromes of the trigeminal, facial and vago-glossopharyngeal nerves: comparative anatomical study of the central myelin portion and transitional zone; correlations with incidences of corresponding hyperactive dysfunctional syndromes. *Acta Neurochir* 2011;153(12):2365–75.
43. Yoshino N, Akimoto H, Yamada I, et al. Trigeminal neuralgia: evaluation of neuralgic manifestation and site of neurovascular compression with 3D CISS MR imaging and MR angiography<sup>1</sup>. *Radiology* 2003;228(2):539–45.
44. Lang E, Naraghi R, Tanrikulu L, et al. Neurovascular relationship at the trigeminal root entry zone in persistent idiopathic facial pain: findings from MRI 3D visualisation. *J Neurol Neurosurg Psychiatr* 2005;76(11):1506–9.
45. Erbay SH, Bhadelia RA, O'Callaghan M, et al. Nerve atrophy in severe trigeminal neuralgia: noninvasive confirmation at MR imaging—initial experience 1. *Radiology* 2006;238(2):689–92.
46. Lutz J, Linn J, Mehrkens JH, et al. Trigeminal neuralgia due to neurovascular compression: high-spatial-resolution diffusion-tensor imaging reveals microstructural neural changes. *Radiology* 2011;258(2):524–30.
47. Yousry I, Moriggl B, Schmid UD, et al. Trigeminal ganglion and its divisions: detailed anatomic MR imaging with contrast-enhanced 3D constructive interference in the steady state sequences. *AJNR Am J Neuroradiol* 2005;26(5):1128–35.
48. Mariniello G, Anecchiarico H, Sardo L, et al. Connections of sympathetic fibres inside the cavernous sinus: a microanatomical study. *Clin Neurol Neurosurg* 2000;102(1):1–5.
49. Williams LS, Schmalfluss IM, Sstrom CL, et al. MR imaging of the trigeminal ganglion, nerve, and the perineural vascular plexus: normal appearance and variants with correlation to cadaver specimens. *AJNR Am J Neuroradiol* 2003;24(7):1317–23.
50. Lang J. *Clinical Anatomy of the Masticatory Apparatus Peripharyngeal Spaces*. New York: G. Thieme Verlag; 1995.
51. Marinkovic SV, Gibo H, Stimec B. The neurovascular relationships and the blood supply of the abducent nerve: surgical anatomy of its cisternal segment. *Neurosurgery* 1994;34(6):1017–26.
52. Lemmerling M, De Praeter G, Mortelet K, et al. Imaging of the normal pontine cisternal segment of the abducens nerve, using three-dimensional constructive interference in the steady state MRI. *Neuroradiology* 1999;41(5):384–6.
53. Yousry I, Camelio S, Wiesmann M, et al. Detailed magnetic resonance imaging anatomy of the cisternal segment of the abducent nerve: Dorello's canal and neurovascular relationships and landmarks. *J Neurosurg* 1999;91(2):276–83.
54. Nathan H, Ouaknine G, Kosary IZ. The abducens nerve. *J Neurosurg* 1974;41(5):561–6.
55. Iaconetta G, Fusco M, Cavallo LM, et al. The abducens nerve: microanatomic and endoscopic study. *Neurosurgery* 2007;61(3):7–14.
56. Alkan A, Sigirci A, Ozveren MF, et al. The cisternal segment of the abducens nerve in man:

- three-dimensional MR imaging. *Eur J Radiol* 2004; 51(3):218–22.
57. Parsa CF, Ellen Grant P, Dillon WP, et al. Absence of the abducens nerve in Duane syndrome verified by magnetic resonance imaging. *Am J Ophthalmol* 1998;125(3):399–401.
  58. Pilyugina SA, Fischbein NJ, Liao YJ, et al. Isolated sixth cranial nerve aplasia visualized with fast imaging employing steady-state acquisition (FIESTA) MRI. *J Neuroophthalmol* 2007;27(2): 127–8.
  59. Ono K, Arai H, Endo T, et al. Detailed MR imaging anatomy of the abducent nerve: evagination of CSF into Dorello canal. *AJNR Am J Neuroradiol* 2004; 25(4):623–6.
  60. Özveren MF, Erol FS, Alkan A, et al. Microanatomical architecture of Dorello's canal and its clinical implications. *Neurosurgery* 2007;60(2):1–8.
  61. Joo W, Yoshioka F, Funaki T, et al. Microsurgical anatomy of the abducens nerve. *Clin Anat* 2012; 25(8):1030–42.
  62. Umansky F, Valarezo A, Elidan J. The microsurgical anatomy of the abducens nerve in its intracranial course. *Laryngoscope* 1992;102(11):1285–92.
  63. Umansky F, Elidan J, Valarezo A. Dorello's canal: a microanatomical study. *J Neurosurg* 1991;75(2): 294–8.
  64. Destrieux C, Velut S, Kakou MK, et al. A new concept in Dorello's canal microanatomy: the petroclival venous confluence. *J Neurosurg* 1997; 87(1):67–72.
  65. Harris FS, Rhoton AL Jr. Anatomy of the cavernous sinus. *J Neurosurg* 1976;45(2):169–80.
  66. Parkinson D, Johnston J, Chaudhuri A. Sympathetic connections to the fifth and sixth cranial nerves. *Anat Rec* 1978;191(2):221–6.